BAMS Map Room

Interactive 3D Visual Analysis of Weather Prediction Data Reveals Midlatitude Overshooting Convection during the CIRRUS-HL Field Experiment

SPECIAL
Waves to Weather (W2W)
COLLECTION

Andreas Schäfler and Marc Rautenhaus

ABSTRACT: In summer 2021, microphysical properties and climate impact of high- and midlatitude ice clouds over Europe and the North Atlantic were studied during the Cirrus High Latitude (CIRRUS-HL) airborne field campaign. The related forecasting and flight planning tasks provided a testbed for interactive 3D visual analysis. Operational analyses and forecasts from the European Centre for Medium-Range Weather Forecasts (ECMWF) were visualized with the open-source software "Met.3D." A combination of traditional 2D displays with innovative 3D views in the interactive visualization framework facilitated rapid and comprehensive exploration of the NWP data. By this means, the benefit of interactive 3D visual forecast products in the routine flight planning procedure was evaluated. Here, we describe the use of 3D tropopause and cloud visualizations during a convective event over the Alps, which became one of the CIRRUS-HL observation targets. For the planning of the research flight on 8 July 2021, our analysis revealed that simulated strong convective updrafts locally disturb the tropopause and inject ice water across the dynamical tropopause into the lower stratosphere. The presented example provides a novel 3D perspective of convective overshooting in a global NWP model and its impact on the tropopause and lower stratosphere. The case study shall encourage the atmospheric science community to further evaluate the use of modern 3D visualization capabilities for NWP analysis.

KEYWORDS: Convective clouds; Stratosphere; Tropopause; Model interpretation and visualization; Forecasting techniques; Field experiments

https://doi.org/10.1175/BAMS-D-22-0103.1
Corresponding author: Andreas Schäfler, andreas.schaefler@dlr.de
Supplemental material: https://doi.org/10.1175/BAMS-D-22-0103.2

In final form 8 May 2023

AFFILIATIONS: Schäfler—Institut für Physik der Atmosphäre, Deutsches Zentrum für Luft- und Raumfahrt, Oberpfaffenhofen, Germany; **Rautenhaus**—Visual Data Analysis Group, Regional Computing Centre, Universität Hamburg, Hamburg, Germany

The careful planning of research flights is of utmost significance for the implementation and success of airborne field campaigns. Such campaigns take place in different parts of the world and, depending on their scientific focus, require specific meteorological conditions. Research aircraft provide in situ observations or curtain-like profile information from remote sensing instruments, observing different parts of the troposphere and lower stratosphere. Flight planning traditionally uses 2D horizontal maps and vertical cross sections of NWP data for the analysis of the forecast conditions (Rautenhaus et al. 2012). Several studies have documented benefits of interactive 3D visualization for NWP analysis, including reduced analysis time and minimizing the risk of missing critical features (Rautenhaus et al. 2018, and references therein).

Our goal for this article is to demonstrate such benefit for flight planning and to discuss how interactive 3D methods facilitate insight into atmospheric processes. We describe some of the experience that we gained during the CIRRUS-HL (https://cirrus-hl.de/) campaign, conducted over Europe and the North Atlantic in summer 2021. As a follow-up of Midlatitude Cirrus (ML-CIRRUS; Voigt et al. 2017), CIRRUS-HL deployed the German research aircraft High Altitude and Long range (HALO) to probe microphysical and radiative properties of ice clouds in high and midlatitudes. For the campaign, we designed and evaluated a set of tailored visual forecast products that combined classical 2D displays with 3D visualizations using operational NWP data from ECMWF. During the analyses of the forecast tropopause, which typically caps the vertical extent of cirrus clouds, we repeatedly noticed regions with a remarkably heterogeneous structure. In this article, to illustrate the use of interactive 3D visualization, we discuss the relation of the heterogeneous tropopause shape to a strong convective event over the Alps and northern Italy that became an observation target on 8 July 2021.

Overshooting convection

One of the goals of CIRRUS-HL was to observe cirrus clouds near the tropopause that originated from convective storms. Thunderstorms are ubiquitous weather systems that occur throughout all latitudes and that are characterized by rising air due to buoyancy with respect to the ambient air. The stratification in the high- to midlatitude troposphere is closely linked to the synoptic-scale flow that can also provide initial trigger mechanisms for convection. When buoyant warm air starts rising in unstable situations, it gains momentum, which is increased by latent heat release in clouds. The ascent proceeds until the convective air reaches the tropopause and pushes into the stably stratified lower stratosphere from where most of the air will return back down. However, modeling and observational studies have shown that midlatitude overshooting convection moistens the lower stratosphere through injection of water vapor and ice (e.g., Dessler and Sherwood 2004; Hegglin et al. 2004; Ray 2004; Mullendore et al. 2005; Homeyer et al. 2014; Homeyer 2015; Smith et al. 2017; Phoenix and Homeyer 2021). The role of convection for the humidity distribution in the stratosphere and its representation in numerical models is an active field of research with many

open questions regarding the transport mechanisms, the amount of moisture that is injected, and the impact of this process in a changing climate (Smith 2021). In this article we provide a 3D illustration of the appearance of overshooting convection and discuss its importance for the tropopause structure as represented in a global NWP model.

Visual analysis setup

Different open-source software can be used for interactive 3D visual analysis of meteorological data [for a list and discussion we refer to the survey by Rautenhaus et al. (2018)]. Here we use "Met.3D" (Rautenhaus et al. 2015a; https://met3d.wavestoweather.de/) that in the past decade has been developed in multiple visualization research projects to investigate novel methods for interactive visual analysis of meteorological simulation data. Originally developed in the context of analyzing ensemble NWP data for flight planning (Rautenhaus et al. 2015b; Schäfler et al. 2018), Met.3D provides typical functionality required for forecasting tasks (e.g., time navigation, ensemble support, and multiple synchronized views). Particularly valuable for us, it follows the concept of "building a bridge" between 2D visual analysis techniques and interactive 3D techniques and embeds classic 2D forecast products frequently used for flight planning in the German atmospheric science community (Rautenhaus et al. 2012; Bauer et al. 2022) in an interactive 3D context. This allows, for example, the structure of 3D atmospheric features (e.g., jet streams, clouds, tropopause, fronts) to be analyzed in relation to planned flight tracks. Met.3D is not limited to flight planning and has evolved into a feature-rich visual analysis tool facilitating rapid and comprehensive exploration of generic atmospheric simulation data; however, its specific NWP analysis approach is unique for our purpose.

During CIRRUS-HL, twice-daily operational forecasts from ECMWF's Integrated Forecasting System (IFS) were transferred to a remote visualization server within computing infrastructure established by the German "Waves to Weather" research program (Craig et al. 2021). The forecasts were obtained at 3-h temporal resolution on a 0.15° grid in both longitude and latitude up to a lead time of 144 h, accounting for the planning horizon of 3–4 days in advance of each flight. The retrieved forecast parameters included 3D [e.g., temperature, wind, pressure, cloud liquid water content (CLWC), cloud ice water content (CIWC)] and 2D fields (e.g., mean sea level pressure, cloud coverage, 6-h accumulated precipitation, and CAPE). In addition, 3D fields of potential temperature (θ), equivalent potential temperature (θ_E) and PV were derived. To locate the tropopause, we used the dynamical tropopause definition based on PV [3.5 PV units (PVU); 1 PVU = 10^{-6} K kg^{-1} m^2 s^{-1}]. Note that different tropopause definitions are used in studies of atmospheric composition (Tinney et al. 2022). Although limitations for quantitative studies of convective mass transport into the stratosphere exist (Maddox and Mullendore 2018) the dynamical tropopause is chosen here as it provides a clear 3D surface that separates the troposphere from the stratosphere.

Classical 2D synoptic overview

We begin our discussion with a classical 2D overview of the synoptic situation, to introduce the concept of a "bridge from 2D to 3D," and to introduce and locate individual weather features that will be referred to in the following 3D analysis. Since interactivity plays a crucial role in the visual analysis process that we describe, the static images presented in this article cannot capture all aspects of the analysis. We hence provide an online supplemental video (https://doi.org/10.1175/BAMS-D-22-0103.2) that captures animated screen recordings that are referenced throughout the article.

Figure 1a shows how at 1500 UTC 8 July 2021, central Europe was affected by an upper-level low off the coast of Norway. An attached southward extending trough, i.e., a cyclonic curvature maximum of the flow, provided large-scale forcing for convection on that day.

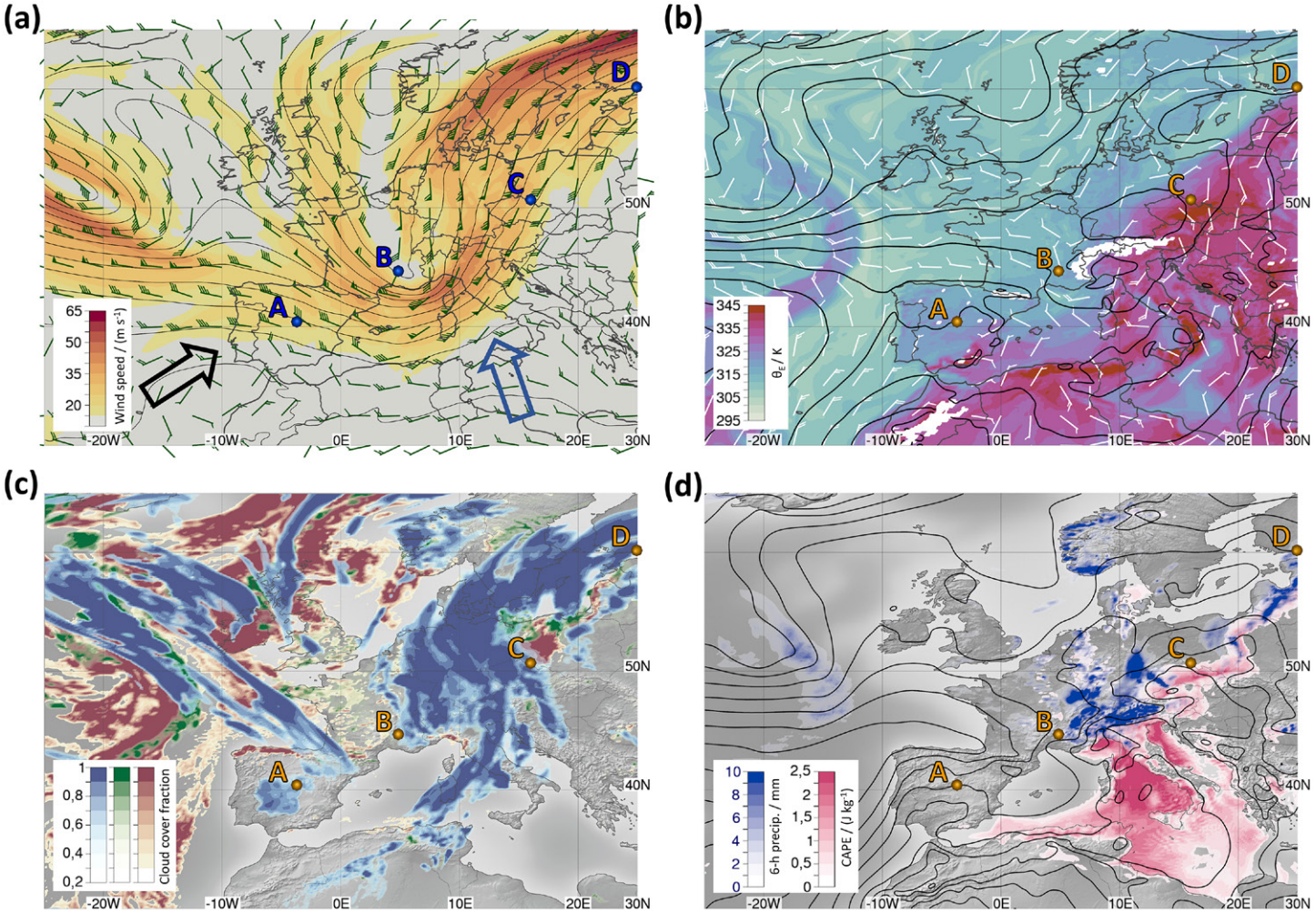

Fig. 1. ECMWF forecast for 1500 UTC 8 Jul 2021 (+15 h): (a) Geopotential height (ΔZ = 40 m; black contours), wind speed (in m s^{-1}; color shading), and wind barbs at 300 hPa. Blue (black) arrow indicates the viewpoint in Fig. 2 (Figs. 3 and 4). (b) Geopotential height (ΔZ = 20 m; black contours), equivalent potential temperature (θ_E; in K; color shading), and wind barbs at 850 hPa. (c) Cloud-cover fraction per grid cell (color shading, with high-level clouds in blue, midlevel clouds in green, low-level clouds in red). (d) Mean sea level pressure (in hPa; Δp = 4 hPa; black contours), 6-h precipitation (mm; blue shading), and CAPE (×10^3 J kg^{-1}; red shading). Labels A–D mark locations of vertical section and poles in Figs. 2–5.

Closer to the ground at 850 hPa, a mesoscale low was located over the Alps (Fig. 1b), with moist and warm air to its southeast as can be seen from increased values of θ_E. Cloud coverage (Fig. 1c, note that clouds at different levels are superimposed when viewed from above) indicates high-level clouds in relation to lifting at the frontal airmass boundaries (Fig. 1b). However, the patchy high-level clouds suggest convective activity in the unstable air beneath (see high CAPE in Fig. 1d), which is confirmed by locally enhanced 6-h precipitation (Fig. 1d). The video (at 00:20 min) shows a time animation of Fig. 1 over 8 July 2021, illustrating the temporal evolution of clouds and precipitation in relation to the northeastward-propagating trough and the stronger convection throughout the day. The relatively early formation of clouds and precipitation suggests an important role of orography for triggering convection over the Alps.

3D exploration of convection and the tropopause

Figure 2 illustrates how 3D information is added as a possible way to analyze upper-level weather charts in a 3D context. The video (at 1 min 20 s; hereafter, video times are given as "MM:SS min") illustrates how viewpoint and location of horizontal and vertical sections were interactively modified during data exploration. For the static images in this

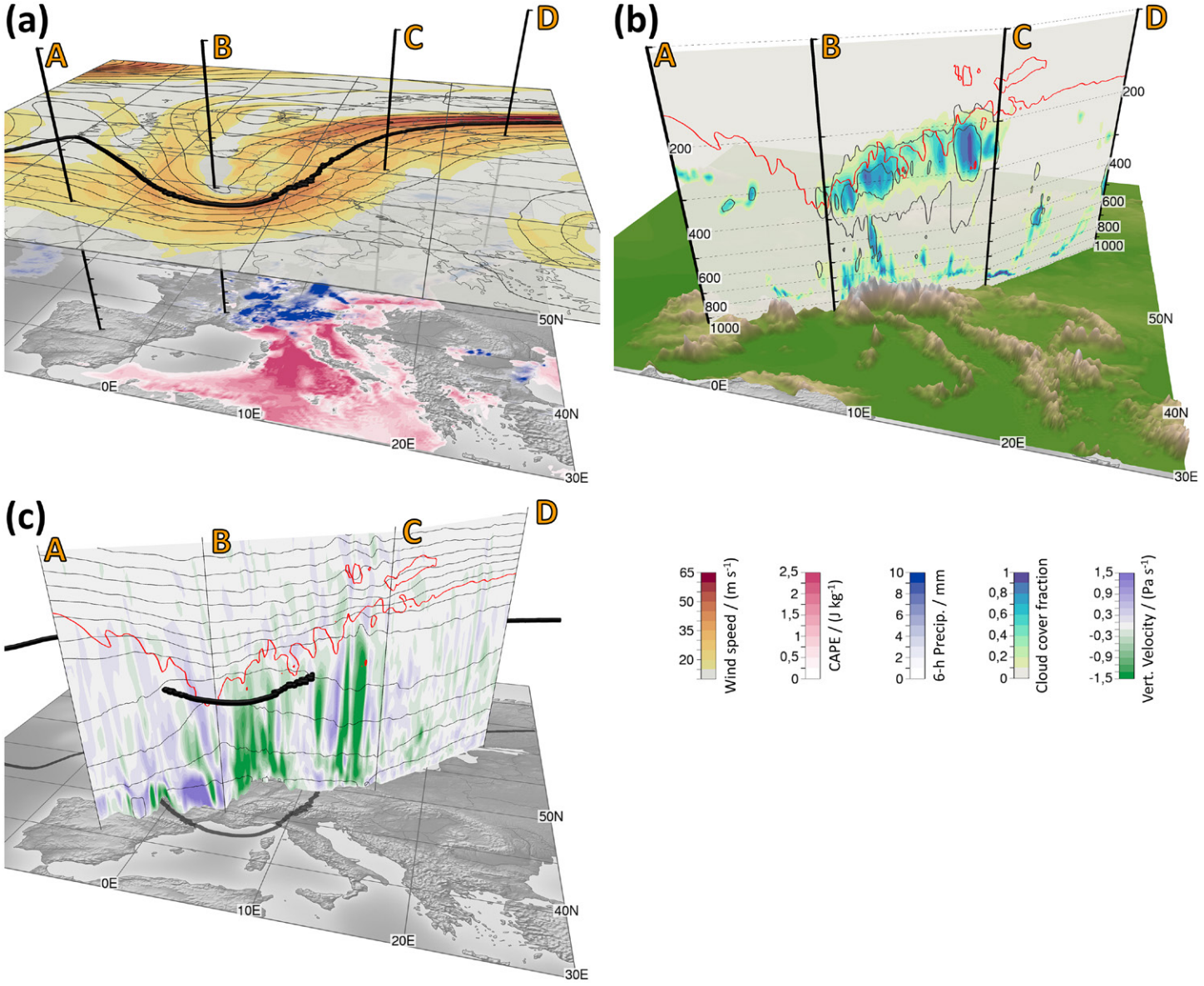

Fig. 2. ECMWF forecast for 1500 UTC 8 Jul 2021 (+15 h): (a) 300 hPa horizontal section of wind speed (in m s^{-1}; color shading), 300 hPa geopotential height (ΔZ = 40 m; black contours, with 9,480 gpm as the thick contour), CAPE (in 10^{-3} J kg^{-1}; pink shading), and 6-h precipitation (mm; blue shading). The four poles (A–D; 1,000–100 hPa; see also Fig. 1) in (a) define the vertical cross sections in (b) and (c). (b) Vertical cross section of cloud-cover fraction per grid cell (0–1; color shading), CIWC (0.01 and 0.1 g kg^{-1}; thick dark gray contours), isobars (dotted lines), and the dynamical tropopause (3.5 PVU; red contour). At the bottom, the ECMWF model topography (as represented by surface pressure) is shown. (c) Vertical cross section of vertical velocity (in Pa s^{-1}; color shading), dynamical tropopause, and potential temperature (thin gray contours). The 9,480 m geopotential height contour at 300 hPa from (a) is shown as a reference.

article, we use the two viewpoints illustrated in Fig. 1a. Figure 2a combines the contents of Figs. 1a and 1d to provide immediate spatial connection between upper-level flow and surface weather, supplemented by four vertical poles (A–D; see also Fig. 1) that, in subsequent plots, span a vertical cross section from central Spain (pole A) to southern Finland (pole D). The Alpine region (between poles B and C) shows increased precipitation and CAPE, with unstable air extending southward over the Mediterranean. A cross section of cloud cover (Fig. 2b) indicates the increased cloud coverage over the Alps (cf. the animated version in the video at 02:22 min), reaching the tropopause at highest altitudes. The tropopause provides the typical decrease in altitude within the cold trough and an ascent toward the warmer air below the anticyclone to the northeast. The tropopause features strong heterogeneity above the clouds and is intersected by CIWC contours.

By displaying vertical velocity on the cross section (Fig. 2c), we can quickly infer that strong convective updrafts are simulated in the unstable air over the Alps leading to cloud formation and precipitation (cf. the video, also at 02:22 min). The stratosphere is characterized by increased static stability as visible from a high density of isentropes.

To analyze how clouds and tropopause shape are intertwined for this event, we apply 3D renderings of cloud distribution and altitude and 3D tropopause structure (Figs. 3 and 4; also compare the supplementary video at 03:08 and 05:20 min). Figure 3a provides an illuminated volume rendering of the forecast clouds, showing extended, banded cirrus clouds over the Atlantic and convective clouds ahead of the trough (note that in all 3D displays the vertical dimension is much exaggerated, approximately by a factor of 60). The heterogenous appearance of the clouds becomes more pronounced in a display of a 3D isosurface of cloud-cover fraction (Fig. 3b) and reflects the strong updrafts within the clouds identified in Fig. 2c.

Figure 4a shows that the tropopause exhibits an extended region of heterogeneities exactly at the same place as the clouds, suggesting a local disturbance by vigorous ascents from the troposphere beneath. To clarify whether water vapor and ice particles were transported into the lower stratosphere in the NWP representation, Fig. 4b combines the tropopause isosurface with a selected CIWC isosurface (0.01 g kg^{-1} as in Fig. 2b). It is clearly visible that CIWC transects the tropopause in the region of strong convective activity, which means that ice is transported above the tropopause. This emerges, in particular, at lower tropopause altitudes at the center of the upper-level trough, confirming findings of Phoenix and Homeyer (2021). No such signal is observed over the Atlantic Ocean in cirrus regions that are driven by large-scale ascent and that exhibit a familiar homogeneous shape of the tropopause above. Finally, Fig. 4c shows that the convective transport across the tropopause leads to increased CIWC at tropopause level. The video highlights that the tropopause heterogeneity and the transport of ice grows with increasing convective activity (at 06:45 min).

Summary and outlook

We illustrated how the combination of traditional 2D displays and 3D visualization in an interactive visual analysis framework enabled rapid exploration of forecast data and contributed to revealing an interesting event. CIRRUS-HL provided an ideal testbed to evaluate

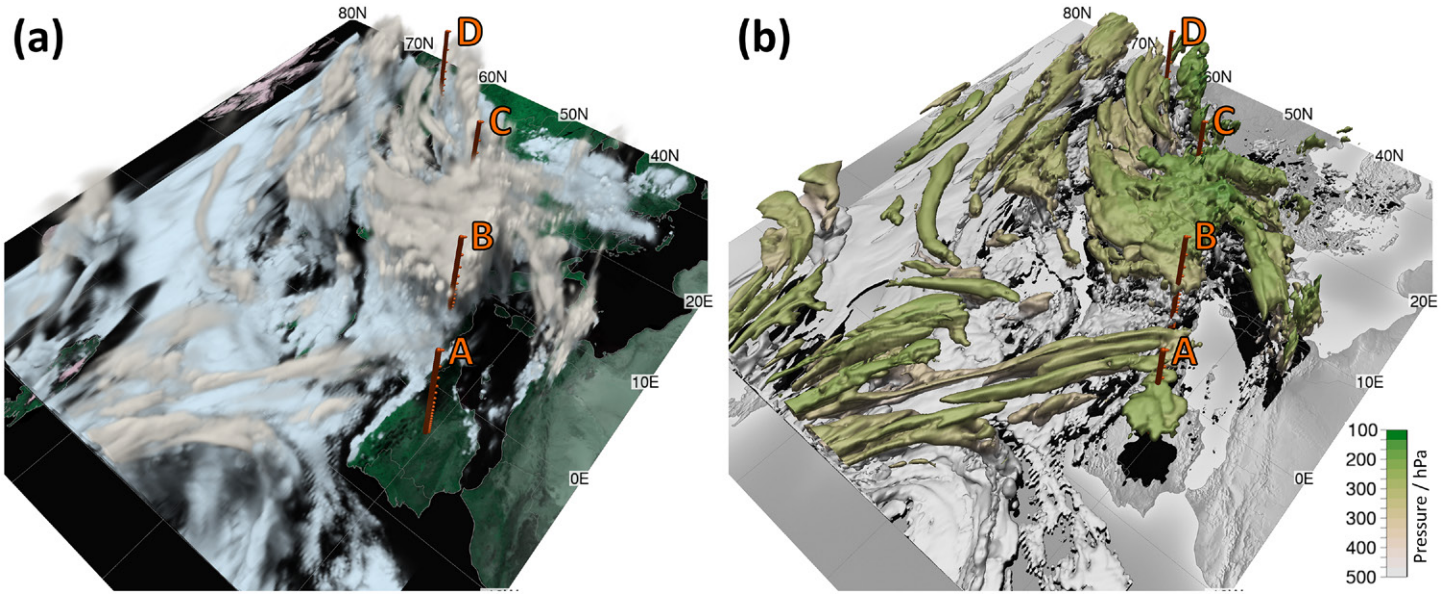

Fig. 3. ECMWF forecast for 1500 UTC 8 Jul 2021 (+15 h): (a) Illuminated volume rendering of CIWC (white) and CLWC (blue). (b) 3D isosurface of cloud-cover fraction per grid cell (>0.3) colored by pressure. Pole locations and labels A–D as shown in Fig. 1.

the routine applicability of interactive 3D visualization for the forecasting tasks for research flight planning. We gathered experience and found that the workflow (illustrated in the supplementary video) is easily accessible to versed meteorologists. The remote visualization infrastructure proved valuable for straightforward use and for collaboration. In conclusion, we are very positive about augmenting 2D displays with interactive 3D elements and continue to use the approach in ongoing and future work. We much encourage readers to gain and share their own experiences in using 3D visualization for forecasting tasks or for understanding and illustrating atmospheric processes.

The effect of convective updrafts on the dynamical tropopause shape was demonstrated earlier, e.g., in high-resolution simulations in Maddox and Mullendore (2018). The 3D analysis presented here highlights the 3D nature of the overshooting process providing a substantial spatial extent of the heterogeneous tropopause and a clear relation to the large-scale synoptic situation. Oertel et al. (2020) have shown that convection embedded in ascending airstreams connected to extratropical cyclones may affect the PV distribution and related synoptic-scale circulation. Hence, a systematic analysis of potential implications for midlatitude weather would be of great interest. Additionally, even though the representation of convection in global NWP models continuously improves, an erroneous moisture transport from the troposphere

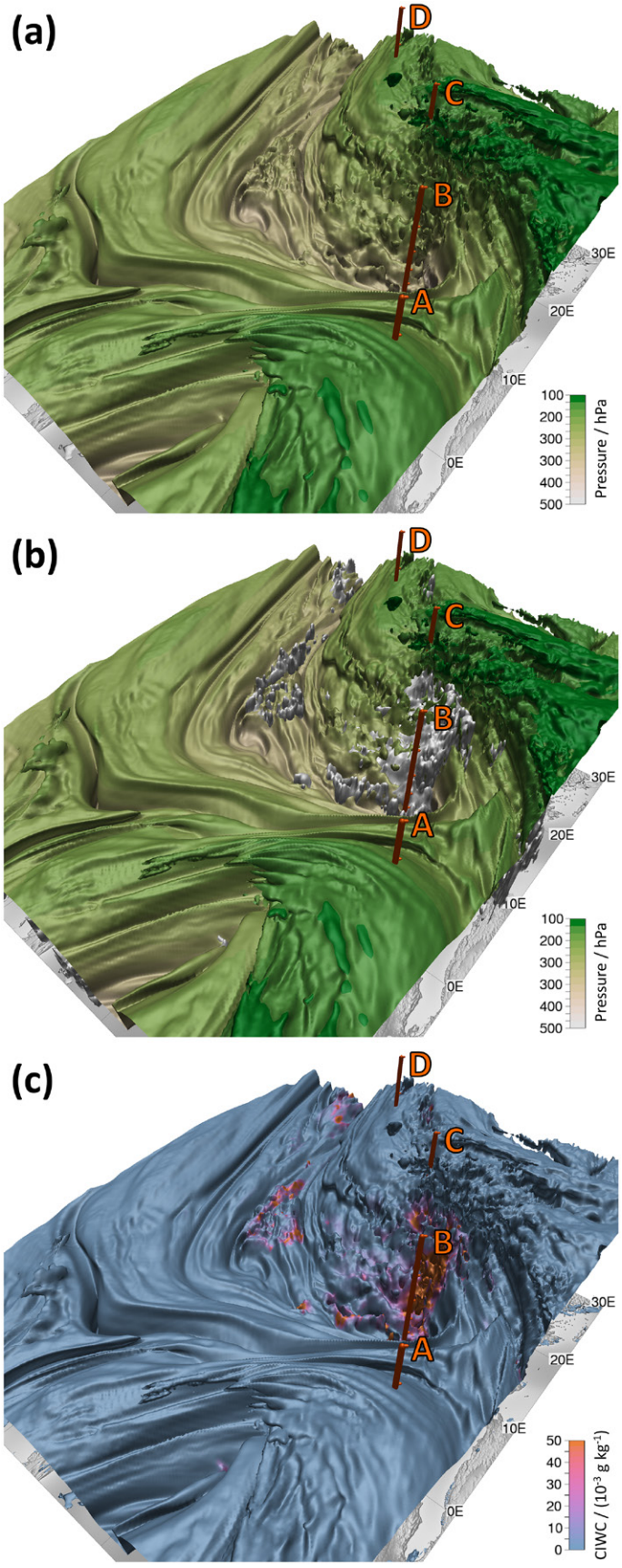

Fig. 4. ECMWF forecast for 1500 UTC 8 Jul 2021 (+15 h): (a) 3D isosurface of the dynamical tropopause (PV = 3.5 PVU) colored by pressure (in hPa). (b) As in (a), but with an additional 3D isosurface of CIWC (white isosurfaces of 0.01 g kg^{-1}). (c) As in (a), but colored by CIWC (×10^{-3} g kg^{-1}). Orange poles (A–D) as shown in Fig. 1.

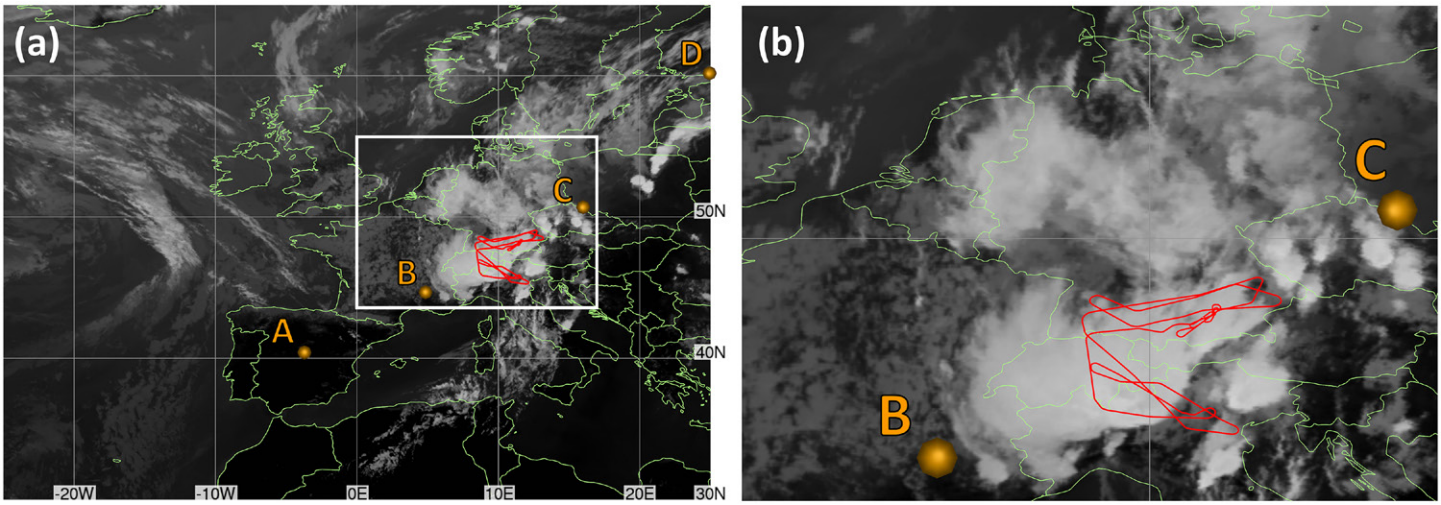

Fig. 5. Meteosat SEVIRI IR 10.8 μm satellite image at 1500 UTC 8 Jul 2021 (from https://view.eumetsat.int/; © EUMETSAT 2022) superimposed by the HALO flight track (red line) between 1300 and 1800 UTC. (b) The subregion enclosed by the white rectangle in (a).

may contribute to the lower stratospheric moist bias that was diagnosed in NWP models (Kaufmann et al. 2018; Krüger et al. 2022).

The presented analysis supported the planning of a HALO research flight in the afternoon of 8 July 2021. The large-scale situation was monitored and compared for successive initialization times using the demonstrated 3D visualizations. After an early convection onset, strong convection was predicted over Switzerland, eastern Austria, and northern Italy toward the evening, forced by the large-scale flow and orographic effects. Interactive exploration with cross sections helped to define flight altitude and legs north and south of the Alps with flight legs in the tropopause region as well as in mixed-phase clouds. The final flight trajectory is shown in Fig. 5; we note that some in-flight modifications were necessary as particularly severe convection over Switzerland prevented flight legs within clouds. The collected observations will be investigated with respect to moisture and ice transport and to moistening of the lower stratosphere. The interpretation of the observations of this and other cases will benefit from analogous 3D visualization.

Acknowledgments. The authors thank the CIRRUS-HL PIs and the weather team for the opportunity to contribute to the flight planning with Met.3D. The authors thank the German Science Foundation (DFG) for supporting this work in the framework of the transregional collaborative research center (SFB/TRR 165) "Waves to Weather" (www.wavestoweather.de). We are grateful to Robert Redl (LMU Munich) for support with the operational data transfer and remote visualization. We thank DWD for granting access to ECMWF forecast data.

Data availability statement. Operational IFS forecast data were retrieved through the ECMWF Meteorological Archival and Retrieval System (MARS). Met.3D is available at https://met3d.wavestoweather.de/.

References

Bauer, R., J.-U. Grooß, J. Ungermann, M. Bär, M. Geldenhuys, and L. Hoffmann, 2022: The Mission Support System (MSS v7.0.4) and its use in planning for the SouthTRAC aircraft campaign. *Geosci. Model Dev.*, **15**, 8983–8997, https://doi.org/10.5194/gmd-15-8983-2022.

Craig, G. C., and Coauthors, 2021: Waves to weather: Exploring the limits of predictability of weather. *Bull. Amer. Meteor. Soc.*, **102**, E2151–E2164, https://doi.org/10.1175/BAMS-D-20-0035.1.

Dessler, A. E., and S. C. Sherwood, 2004: Effect of convection on the summertime extratropical lower stratosphere. *J. Geophys. Res.*, **109**, D23301, https://doi.org/10.1029/2004JD005209.

Hegglin, M. I., and Coauthors, 2004: Tracing troposphere-to-stratosphere transport above a mid-latitude deep convective system. *Atmos. Chem. Phys.*, **4**, 741–756, https://doi.org/10.5194/acp-4-741-2004.

Homeyer, C. R., 2015: Numerical simulations of extratropical tropopause-penetrating convection: Sensitivities to grid resolution. *J. Geophys. Res. Atmos.*, **120**, 7174–7188, https://doi.org/10.1002/2015JD023356.

——, and Coauthors, 2014: Convective transport of water vapor into the lower stratosphere observed during double-tropopause events. *J. Geophys. Res. Atmos.*, **119**, 10 941–10 958, https://doi.org/10.1002/2014JD021485.

Kaufmann, S., and Coauthors, 2018: Intercomparison of midlatitude tropospheric and lower-stratospheric water vapor measurements and comparison to ECMWF humidity data. *Atmos. Chem. Phys.*, **18**, 16 729–16 745, https://doi.org/10.5194/acp-18-16729-2018.

Krüger, K., A. Schäfler, M. Wirth, M. Weissmann, and G. Craig, 2022: Vertical structure of the lower-stratospheric moist bias in the ERA5 reanalysis and its connection to mixing processes. *Atmos. Chem. Phys.*, **22**, 15 559–15 577, https://doi.org/10.5194/acp-22-15559-2022.

Maddox, E. M., and G. L. Mullendore, 2018: Determination of best tropopause definition for convective transport studies. *J. Atmos. Sci.*, **75**, 3433–3446, https://doi.org/10.1175/JAS-D-18-0032.1.

Mullendore, G. L., D. R. Durran, and J. R. Holton, 2005: Cross-tropopause tracer transport in midlatitude convection. *J. Geophys. Res.*, **110**, D06113, https://doi.org/10.1029/2004JD005059.

Oertel, A., M. Boettcher, H. Joos, M. Sprenger, and H. Wernli, 2020: Potential vorticity structure of embedded convection in a warm conveyor belt and its relevance for large-scale dynamics. *Wea. Climate Dyn.*, **1**, 127–153, https://doi.org/10.5194/wcd-1-127-2020.

Phoenix, D. B., and C. R. Homeyer, 2021: Simulated impacts of tropopause-overshooting convection on the chemical composition of the upper troposphere and lower stratosphere. *J. Geophys. Res. Atmos.*, **126**, e2021JD034568, https://doi.org/10.1029/2021JD034568.

Rautenhaus, M., G. Bauer, and A. Dörnbrack, 2012: A web service based tool to plan atmospheric research flights. *Geosci. Model Dev.*, **5**, 55–71, https://doi.org/10.5194/gmd-5-55-2012.

——, M. Kern, A. Schäfler, and R. Westermann, 2015a: Three-dimensional visualization of ensemble weather forecasts—Part 1: The visualization tool Met.3D (version 1.0). *Geosci. Model Dev.*, **8**, 2329–2353, https://doi.org/10.5194/gmd-8-2329-2015.

——, C. M. Grams, A. Schäfler, and R. Westermann, 2015b: Three-dimensional visualization of ensemble weather forecasts—Part 2: Forecasting warm conveyor belt situations for aircraft-based field campaigns. *Geosci. Model Dev.*, **8**, 2355–2377, https://doi.org/10.5194/gmd-8-2355-2015.

——, M. Böttinger, S. Siemen, R. Hoffman, R. M. Kirby, M. Mirzargar, N. Röber, and R. Westermann, 2018: Visualization in meteorology—A survey of techniques and tools for data analysis tasks. *IEEE Trans. Visualization Comput. Graphics*, **24**, 3268–3296, https://doi.org/10.1109/TVCG.2017.2779501.

Ray, E. A., 2004: Evidence of the effect of summertime midlatitude convection on the subtropical lower stratosphere from CRYSTAL-FACE tracer measurements. *J. Geophys. Res.*, **109**, D18304, https://doi.org/10.1029/2004JD004655.

Schäfler, A., and Coauthors, 2018: The North Atlantic Waveguide and Downstream Impact Experiment. *Bull. Amer. Meteor. Soc.*, **99**, 1607–1637, https://doi.org/10.1175/BAMS-D-17-0003.1.

Smith, J. B., 2021: Convective hydration of the stratosphere. *Science*, **373**, 1194–1195, https://doi.org/10.1126/science.abl8740.

——, and Coauthors, 2017: A case study of convectively sourced water vapor observed in the overworld stratosphere over the United States. *J. Geophys. Res. Atmos.*, **122**, 9529–9554, https://doi.org/10.1002/2017JD026831.

Tinney, E. N., C. R. Homeyer, L. Elizalde, D. F. Hurst, A. M. Thompson, R. M. Stauffer, H. Vömel, and H. B. Selkirk, 2022: A modern approach to stability-based definition of the tropopause. *Mon. Wea. Rev.*, **150**, 3151–3174, https://doi.org/10.1175/MWR-D-22-0174.1.

Voigt, C., and Coauthors, 2017: ML-CIRRUS: The airborne experiment on natural cirrus and contrail cirrus with the high-altitude long-range research aircraft HALO. *Bull. Amer. Meteor. Soc.*, **98**, 271–288, https://doi.org/10.1175/BAMS-D-15-00213.1.